Absolute Quantum Yield for Understanding the Upconversion and Downshift Properties of Luminescent PbF_2:Er^{3+},Yb^{3+} Crystals

Eduard Madirov, Dmitry Busko, Ian A. Howard, Bryce S. Richards and Andrey Turshatov

Table S1. Integrated absorption cross-section of the PbF_2:Er^{3+}, Yb^{3+} samples used in the Judd-Ofelt calculations, $\times 10^{-20}$ cm^2

	Er1.5Yb1.5	Er2Yb2	Er2Yb3	Er2Yb5	Er2Yb7
$^4G_{11/2}$	5.982	6.628	6.628	6.757	7.825
$^2H_{9/2}$	0.620	0.877	0.853	0.789	0.988
$^4F_{7/2}$	2.797	3.860	3.911	3.931	4.782
$^2H_{11/2}$	6.099	6.860	6.715	6.747	8.450
$^4S_{3/2}$	0.972	1.649	1.361	1.293	1.727
$^4F_{9/2}$	5.624	7.443	7.789	7.964	9.657
$^4I_{13/2}$	34.724	41.620	42.104	44.380	54.139

Table S2. Concentrations of the doping ions based on WDXRF and ions per cm^3, unit cell parameters of the PbF_2 doped with Er^{3+}, Yb^{3+}.

Sample name	Er^{3+}		Yb^{3+}		a, Å
	mol.,%	N, $\times 10^{20}$cm^{-3}	mol.,%	N, $\times 10^{20}$cm^{-3}	
Er1.5Yb1.5	1.61	3.34	1.436	2.98	5.9301
Er2Yb2	2.106	4.36	2.141	4.44	5.9236
Er2Yb3	2.186	4.53	3.285	6.81	5.9174
Er2Yb5	2.116	4.38	5.142	10.66	5.9078
Er2Yb7.5	2.116	4,38	7.713	15,99	5.8887

Table S3. Predicted radiative lifetimes and branching ratios of some transitions in the Er1.5Yb1.5 sample.

	E1, cm^{-1}	E2, cm^{-1}	ΔE, cm^{-1}	A, s^{-1}	β	τ_{rad}, ms
$^2H_{9/2} - {}^2H_{11/2}$	24756	19337	5419	18.634	0.0140	0.751
$- {}^4F_{9/2}$	24756	15455	9301	41.471	0.0311	
$- {}^4I_{11/2}$	24756	10346	14410	118.013	0.0886	
$- {}^4I_{13/2}$	24756	6712	18044	542.343	0.407	
$- {}^4I_{15/2}$	24756	217	24539	611.763	0.459	
$^2H_{11/2} - {}^4I_{13/2}$	19337	6712	12625	41.151	0.0282	0.686
$- {}^4I_{15/2}$	19337	217	19120	1416.983	0.972	
$^4S_{3/2} - {}^4F_{9/2}$	18583	15455	3128	0.3421	3.818E-4	1.116
$- {}^4I_{9/2}$	18583	12597	5986	30.958	0.0345	
$- {}^4I_{11/2}$	18583	10346	8237	19.825	0.0221	
$- {}^4I_{13/2}$	18583	6712	11871	247.769	0.277	
$- {}^4I_{15/2}$	18583	217	18366	597.118	0.666	
$^4F_{9/2} - {}^4I_{9/2}$	15455	12597	2858	0.726	0.00117	1.468
$- {}^4I_{11/2}$	15455	10346	5109	31.586	0.0464	
$- {}^4I_{13/2}$	15455	6712	8743	28.874	0.0424	
$- {}^4I_{15/2}$	15455	217	15238	620.141	0.9102	
$^4I_{9/2} - {}^4I_{11/2}$	12597	10346	2251	3.319	0.0399	12.033
$- {}^4I_{13/2}$	12597	6712	5885	25.395	0.306	
$- {}^4I_{15/2}$	12597	217	12380	54.392	0.654	
$^4I_{11/2} - {}^4I_{13/2}$	10346	6712	3634	22.446	0.259	11.517
$- {}^4I_{15/2}$	10346	217	10129	64.383	0.741	
$^4I_{13/2} - {}^4I_{15/2}$	6712	217	6495	103.025	1	9.706

Table S4. Predicted radiative lifetimes and branching ratios of some transitions in the Er2Yb2 sample.

	E1, cm^{-1}	**E2, cm^{-1}**	**ΔE, cm^{-1}**	**A, s^{-1}**	**β**	τ_{rad}**, ms**
$^2H_{9/2}$ – $^2H_{11/2}$	24756	19337	5419	20.613	0.0121	0.588
– $^4F_{9/2}$	24756	15455	9301	45.873	0.0270	
– $^4I_{11/2}$	24756	10346	14410	146.500	0.0862	
– $^4I_{13/2}$	24756	6712	18044	685.112	0.403	
– $^4I_{15/2}$	24756	217	24539	801.826	0.471	
$^2H_{11/2}$ – $^4I_{13/2}$	19337	6712	12625	51.242	0.0323	0.629
– $^4I_{15/2}$	19337	217	19120	1537.217	0.968	
$^4S_{3/2}$ – $^4F_{9/2}$	18583	15455	3128	0.447	3.817E-4	0.853
– $^4I_{9/2}$	18583	12597	5986	40.692	0.0347	
– $^4I_{11/2}$	18583	10346	8237	25.958	0.0221	
– $^4I_{13/2}$	18583	6712	11871	324.008	0.276	
– $^4I_{15/2}$	18583	217	18366	780.852	0.666	
$^4F_{9/2}$ – $^4I_{9/2}$	15455	12597	2858	0.726	8.072E-4	1.111
– $^4I_{11/2}$	15455	10346	5109	40.562	0.0451	
– $^4I_{13/2}$	15455	6712	8743	37.706	0.0419	
– $^4I_{15/2}$	15455	217	15238	820.850	0.912	
$^4I_{9/2}$ – $^4I_{11/2}$	12597	10346	2251	3.457	0.0316	9.147
– $^4I_{13/2}$	12597	6712	5885	33.213	0.304	
– $^4I_{15/2}$	12597	217	12380	72.657	0.665	
$^4I_{11/2}$ – $^4I_{13/2}$	10346	6712	3634	25.155	0.234	9.305
– $^4I_{15/2}$	10346	217	10129	82.314	0.766	
$^4I_{13/2}$ – $^4I_{15/2}$	6712	217	6495	119.264	1	8.385

Table S5. Predicted radiative lifetimes and branching ratios of some transitions in the Er2Yb3 sample.

	E1, cm^{-1}	E2, cm^{-1}	ΔE, cm^{-1}	A, s^{-1}	β	τ_{rad}, ms
$^2H_{9/2} - {}^2H_{11/2}$	24756	19337	5419	20.971	0.0121	0.561
$- {}^4F_{9/2}$	24756	15455	9301	46.741	0.0262	
$- {}^4I_{11/2}$	24756	10346	14410	152.445	0.0854	
$- {}^4I_{13/2}$	24756	6712	18044	717.234	0.402	
$- {}^4I_{15/2}$	24756	217	24539	846.532	0.474	
$^2H_{11/2} - {}^4I_{13/2}$	19337	6712	12625	53.226	0.0330	0.621
$- {}^4I_{15/2}$	19337	217	19120	1558.149	0.967	
$^4S_{3/2} - {}^4F_{9/2}$	18583	15455	3128	0.473	3.817E-4	0.807
$- {}^4I_{9/2}$	18583	12597	5986	42.869	0.0346	
$- {}^4I_{11/2}$	18583	10346	8237	27.426	0.0221	
$- {}^4I_{13/2}$	18583	6712	11871	342.655	0.277	
$- {}^4I_{15/2}$	18583	217	18366	825.792	0.666	
$^4F_{9/2} - {}^4I_{9/2}$	15455	12597	2858	0.728	7.720E-4	1.060
$- {}^4I_{11/2}$	15455	10346	5109	42.759	0.0453	
$- {}^4I_{13/2}$	15455	6712	8743	39.364	0.0417	
$- {}^4I_{15/2}$	15455	217	15238	860.269	0.912	
$^4I_{9/2} - {}^4I_{11/2}$	12597	10346	2251	3.487	0.0305	8.754
$- {}^4I_{13/2}$	12597	6712	5885	35.116	0.307	
$- {}^4I_{15/2}$	12597	217	12380	75.630	0.662	
$^4I_{11/2} - {}^4I_{13/2}$	10346	6712	3634	25.785	0.229	8.889
$- {}^4I_{15/2}$	10346	217	10129	86.719	0.771	
$^4I_{13/2} - {}^4I_{15/2}$	6712	217	6495	123.125	1	8.122

Table S6. Predicted radiative lifetimes and branching ratios of some transitions in the Er2Yb5 sample.

	E1, cm^{-1}	E2, cm^{-1}	ΔE, cm^{-1}	A, s^{-1}	β	τ_{rad}, ms
$^2H_{9/2} - ^2H_{11/2}$	24756	19337	5419	21.339	0.012	0.562
$- ^4F_{9/2}$	24756	15455	9301	46.813	0.0263	
$- ^4I_{11/2}$	24756	10346	14410	154.156	0.0872	
$- ^4I_{13/2}$	24756	6712	18044	716.779	0.402	
$- ^4I_{15/2}$	24756	217	24539	839.599	0.472	
$^2H_{11/2} - ^4I_{13/2}$	19337	6712	12625	54.359	0.0343	0.617
$- ^4I_{15/2}$	19337	217	19120	1567.031	0.966	
$^4S_{3/2} - ^4F_{9/2}$	18583	15455	3128	0.465	3.816E-4	0.820
$- ^4I_{9/2}$	18583	12597	5986	42.997	0.0356	
$- ^4I_{11/2}$	18583	10346	8237	27.092	0.0221	
$- ^4I_{13/2}$	18583	6712	11871	336.800	0.276	
$- ^4I_{15/2}$	18583	217	18366	811.681	0.666	
$^4F_{9/2} - ^4I_{9/2}$	15455	12597	2858	0.708	7.303E-4	1.031
$- ^4I_{11/2}$	15455	10346	5109	42.022	0.0432	
$- ^4I_{13/2}$	15455	6712	8743	40.814	0.0428	
$- ^4I_{15/2}$	15455	217	15238	886.471	0.914	
$^4I_{9/2} - ^4I_{11/2}$	12597	10346	2251	3.493	0.0291	8.424
$- ^4I_{13/2}$	12597	6712	5885	34.553	0.291	
$- ^4I_{15/2}$	12597	217	12380	80.655	0.679	
$^4I_{11/2} - ^4I_{13/2}$	10346	6712	3634	25.712	0.232	9.020
$- ^4I_{15/2}$	10346	217	10129	85.155	0.768	
$^4I_{13/2} - ^4I_{15/2}$	6712	217	6495	122.337	1	8.174

Table S7. Predicted radiative lifetimes and branching ratios of some transitions in the Er2Yb7.5 sample.

	E1, cm^{-1}	E2, cm^{-1}	ΔE, cm^{-1}	A, s^{-1}	β	τ_{rad}, ms
$^2H_{9/2} - {}^2H_{11/2}$	24756	19337	5419	23.065	0.0106	0.445
$- {}^4F_{9/2}$	24756	15455	9301	59.028	0.0262	
$- {}^4I_{11/2}$	24756	10346	14410	190.396	0.0855	
$- {}^4I_{13/2}$	24756	6712	18044	903.994	0.402	
$- {}^4I_{15/2}$	24756	217	24539	1072.468	0.477	
$^2H_{11/2} - {}^4I_{13/2}$	19337	6712	12625	65.929	0.0327	0.493
$- {}^4I_{15/2}$	19337	217	19120	1962.310	0.967	
$^4S_{3/2} - {}^4F_{9/2}$	18583	15455	3128	0.603	3.819E-4	0.633
$- {}^4I_{9/2}$	18583	12597	5986	53.822	0.0346	
$- {}^4I_{11/2}$	18583	10346	8237	34.857	0.022	
$- {}^4I_{13/2}$	18583	6712	11871	437.221	0.277	
$- {}^4I_{15/2}$	18583	217	18366	1053.695	0.667	
$^4F_{9/2} - {}^4I_{9/2}$	15455	12597	2858	0.943	8.138E-4	0.862
$- {}^4I_{11/2}$	15455	10346	5109	54.590	0.0471	
$- {}^4I_{13/2}$	15455	6712	8743	48.078	0.0413	
$- {}^4I_{15/2}$	15455	217	15238	1055.930	0.910	
$^4I_{9/2} - {}^4I_{11/2}$	12597	10346	2251	3.638	0.0264	7.222
$- {}^4I_{13/2}$	12597	6712	5885	44.770	0.323	
$- {}^4I_{15/2}$	12597	217	12380	90.052	0.650	
$^4I_{11/2} - {}^4I_{13/2}$	10346	6712	3634	29.061	0.207	7.150
$- {}^4I_{15/2}$	10346	217	10129	110.796	0.792	
$^4I_{13/2} - {}^4I_{15/2}$	6712	217	6495	142.934	1	6.996

Table S8. Decay times obtained after fitting the experimental decays in Figures 3b-3d with single-exponential ($^4I_{13/2}$-$^4I_{15/2}$ and $^4F_{9/2}$-$^4I_{15/2}$ transitions) and bi-exponential ($^4S_{1/2}$-$^4I_{15/2}$ transition) functions.

$^4I_{13/2}$-$^4I_{15/2}$	
crystal	**τ, ms**
Er1.5Yb1.5	11.0±0.5
Er2Yb2	7.8±0.4
Er2Yb3	8.2±0.4
Er2Yb5	8.8±0.4
Er2Yb7.5	8.9±0.4

$^4F_{9/2}$-$^4I_{15/2}$	
crystal	**τ, ms**
Er1.5Yb1.5	0.44±0.05
Er2Yb2	0.36±0.04
Er2Yb3	0.38±0.04
Er2Yb5	0.36±0.04
Er2Yb7.5	0.37±0.04

$^4S_{1/2}$-$^4I_{15/2}$				
crystal	**τ_1, ms**	**A_1**	**τ_2, ms**	**A_2**
Er1.5Yb1.5	0.18±0.04	0.37	1.08±0.24	0.58
Er2Yb2	0.08±0.02	0.94	0.94±0.21	0.12
Er2Yb3	0.06±0.01	1.00	0.64±0.14	0.08
Er2Yb5	0.05±0.01	0.96	0.56±0.13	0.05
Er2Yb7.5	0.04±0.01	1.01	0.25±0.06	0.03

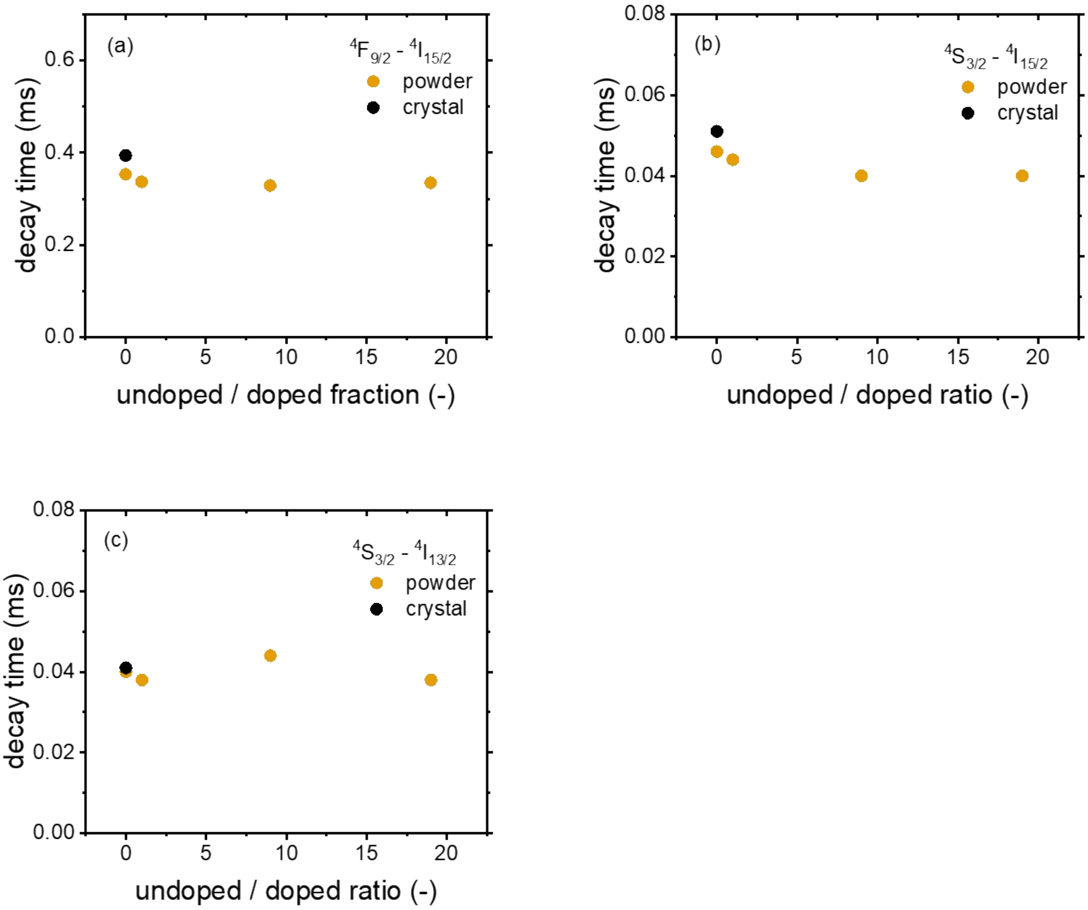

Figure S1 Luminescence decay times of the Er^{3+}:$^4S_{3/2}$ – $^4I_{15/2}$, Er^{3+}:$^4S_{3/2}$ – $^4I_{13/2}$, Er^{3+}:$^4F_{9/2}$ – $^4I_{15/2}$ transitions of the Er2Yb5 crystal and diluted powders.

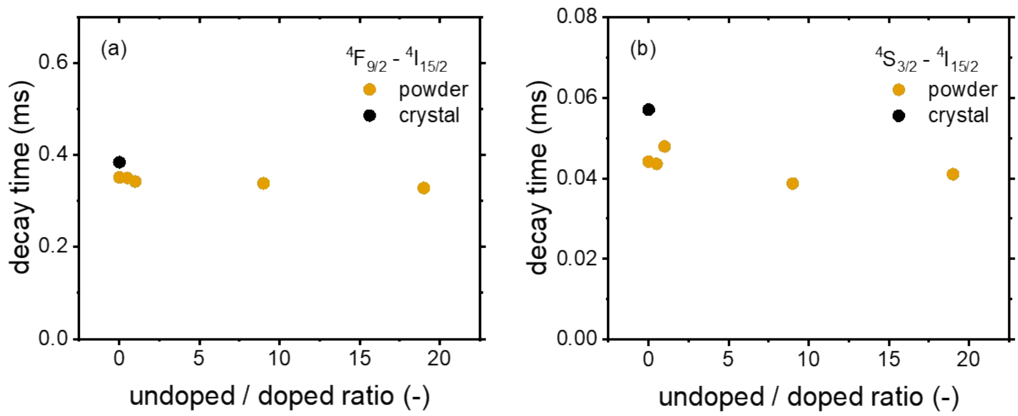

Figure S2. Luminescence decay times of the Er^{3+}:$^4S_{3/2}$ – $^4I_{15/2}$ and Er^{3+}:$^4F_{9/2}$ – $^4I_{15/2}$ transitions of the Er2Yb2 crystal and diluted powders.

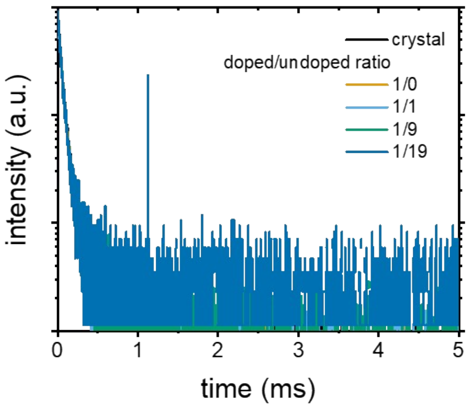

Figure S3. Lumenescence decay of the Er^{3+}:$^4S_{3/2} - {}^4I_{13/2}$ of the Er2Yb5 crystal and diluted powders under 522 nm excitation.

Table S9. Experimentally obtained ϕ_{DS}^{*} (%) of some transitions in the PbF_2:Er^{3+}, Yb^{3+} samples upon excitation of the $^4S_{3/2}$, $^4F_{9/2,}$ Er^{3+}:$^4I_{11/2}$ & Yb^{3+}:$^2F_{7/2}$ and $^4I_{13/2}$ levels as measured in an integrating sphere.

Excitation	Emission	Er1.5Yb1.5	Er2Yb2	Er2Yb3	Er2Yb5	Er2Yb7.5
522 nm 0.1 W/cm^2	$^4S_{3/2}$ – $^4I_{15/2}$	4.4	2.6	2.9	2.6	1.9
	$^4S_{3/2}$ – $^4I_{13/2}$	2	1.2	1.5	1.3	0.9
	$^4F_{9/2}$ – $^4I_{15/2}$	7	6.3	5.6	3.5	1.1
	{Er^{3+}:$^4I_{11/2}$ & Yb^{3+}:$^2F_{7/2}$}	38.2	40	43.9	36.1	30.1
652 nm 0.3 W/cm^2	$^4F_{9/2}$ – $^4I_{15/2}$	18.3	20.1	23.5	22	16.6
	{Er^{3+}:$^4I_{11/2}$ & Yb^{3+}:$^2F_{7/2}$}	22.8	22.5	21.3	20.1	12.2
940 nm 0.1 W/cm^2	{Er^{3+}:$^4I_{11/2}$ & Yb^{3+}:$^2F_{7/2}$}	29.6	48.8	57.2	40.5	31.2
	$^4I_{13/2}$– $^4I_{15/2}$	3.5	3.1	3.2	2.1	1.9
1495 nm 0.1 W/cm^2	$^4I_{13/2}$– $^4I_{15/2}$	83.2	67.2	61.4	62.4	59.1

The correction of the measured ϕ_{DS} values for reabsorption was performed as follows (by analogy with to C. de Mello Donegá et al[1].): a part of every crystal was ground to powder in a mortar and then the obtained powders were diluted with $BaSO_4$ in the ration of 9/1 where the first number is the fraction of $BaSO_4$ and the second one is the fraction of PbF_2 powder. Then spectra of every single crystal and diluted powder were obtained under 378 nm excitation with a spectrofluorometer (FS5, Edinburgh Instruments) in the visible and NIR ranges. The visible emission was normalised to the peak of the $^4S_{3/2}$ - $^4I_{13/2}$ transition at 850 nm. In the case of NIR emission bands, each band was normalised to the long wavelength edge (1585 nm in the case of $^4I_{13/2}$ - $^4I_{15/2}$ emission and 1045 nm in the case of {Er^{3+}:$^4I_{11/2}$ & Yb^{3+}:$^2F_{7/2}$} emission). The corrected ϕ_{DS} values were obtained according to Wilson and Richards[2] as

$$\phi_{DS} = \frac{\phi_{DS}^{*}}{1 - a + a * \phi_{DS}}$$

Where $a = 1 - \frac{\int I_{crystal} d\lambda}{\int I_{powder} d\lambda}$, $I_{crystal}$ is the normalized emission intensity of a single crystal sample, I_{powder} is the normalized emission intensity of a 9/1 diluted powder sample. The integration ranges are 500 – 580 nm for the combination of $^4S_{3/2}$ – $^4I_{15/2}$ and $^2H_{11/2}$ – $^4I_{15/2}$ bands, 610 – 705 nm for the $^4F_{9/2}$ –

$^4I_{15/2}$ emission, 920 – 1100 nm for the {Er^{3+}:$^4I_{11/2}$ & Yb^{3+}:$^2F_{7/2}$} band and 1430 – 1700 nm for the $^4I_{13/2}$–$^4I_{15/2}$ emission band.

The spectra that were used for the calculations are presented in **figure S4.1-3**.

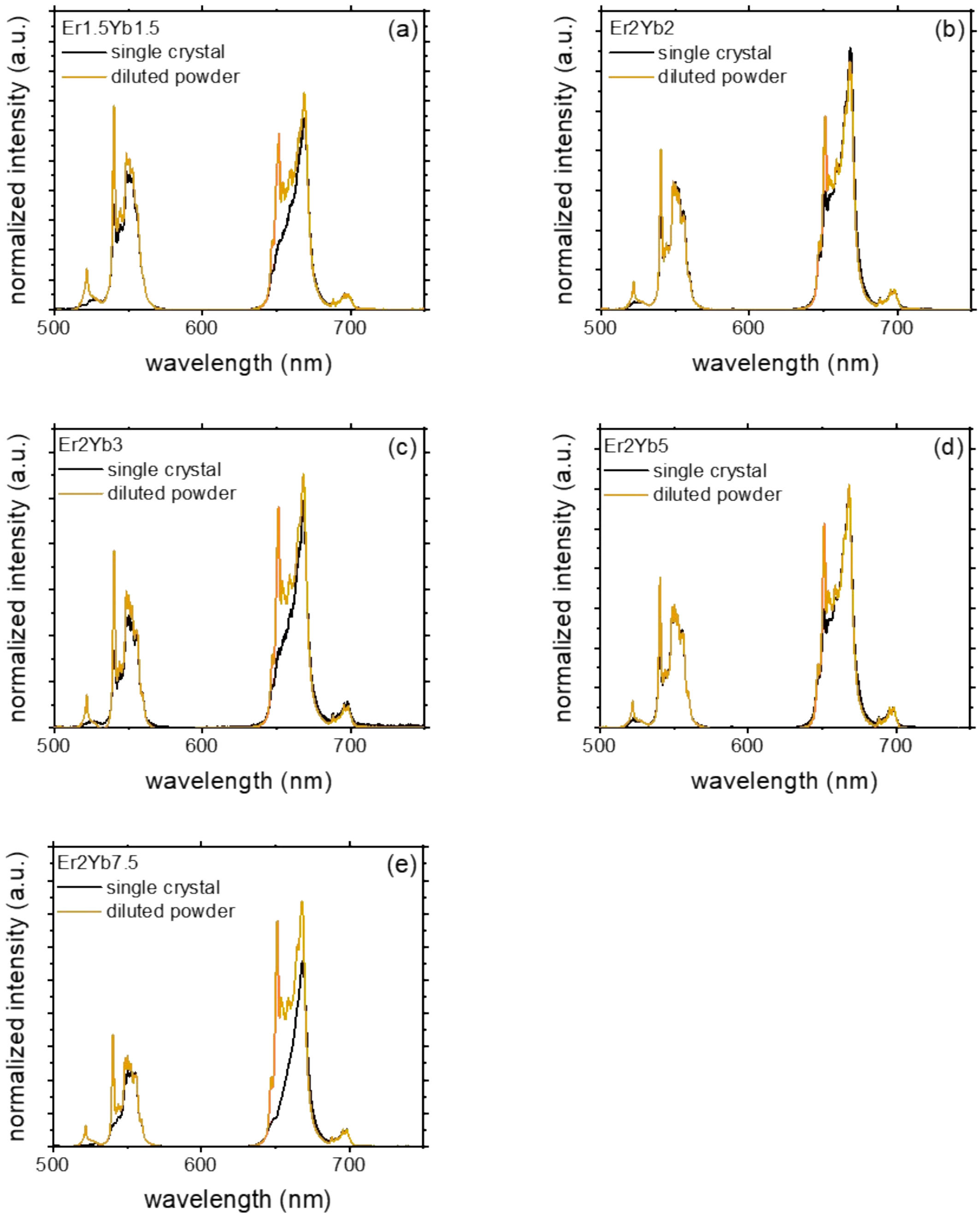

Figure S4.1. Visible range emission spectra of the single crystals and 9/1 diluted powders of the PbF_2:Er,Yb samples measured under 378 nm excitation with a spectrofluorometer (FS5, Edinburgh Instruments).

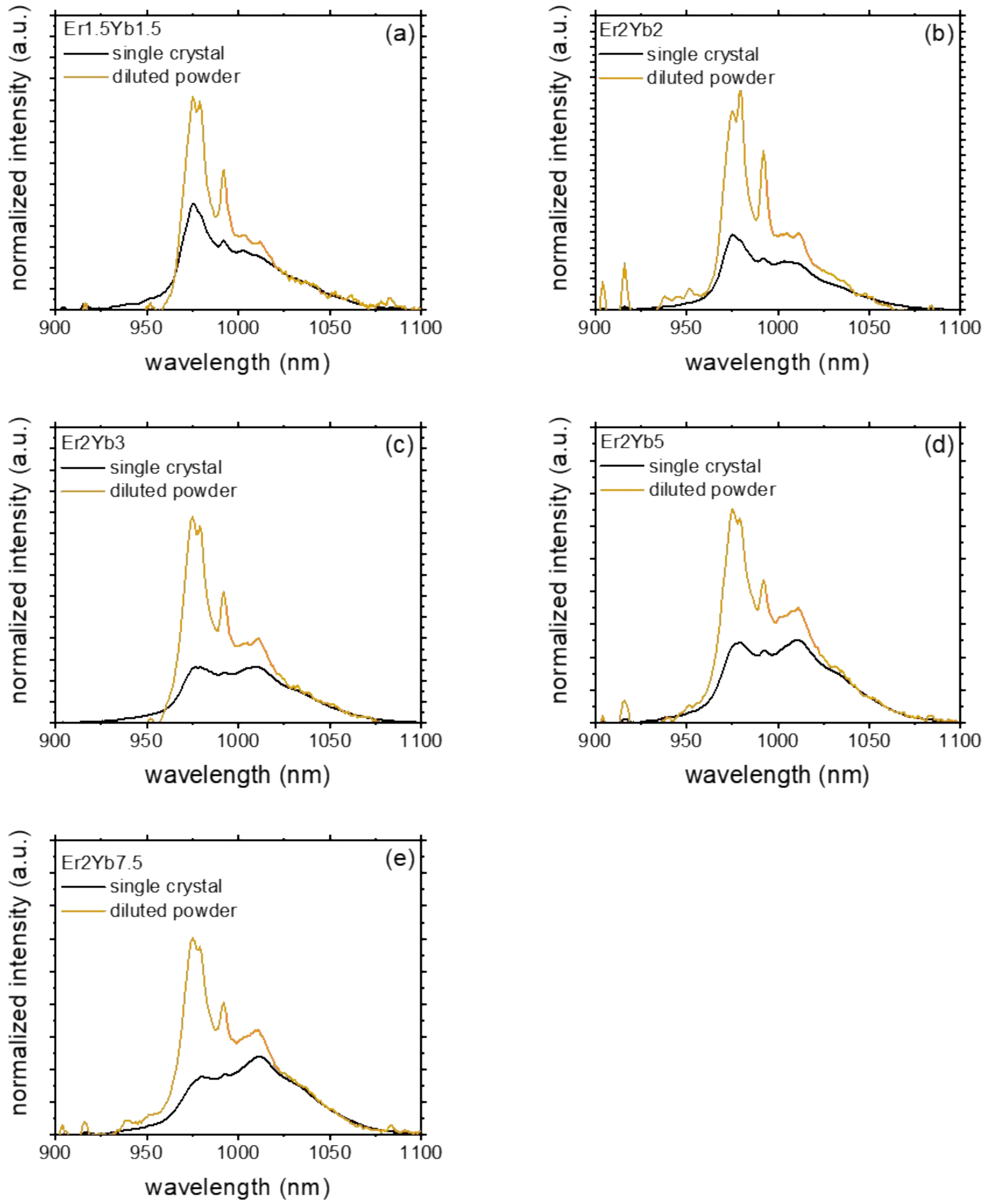

Figure S4.2. NIR range emission spectra of the single crystals and 9/1 diluted powders of the PbF_2:Er,Yb samples measured under 378 nm excitation with a spectrofluorometer (FS5, Edinburgh Instruments).

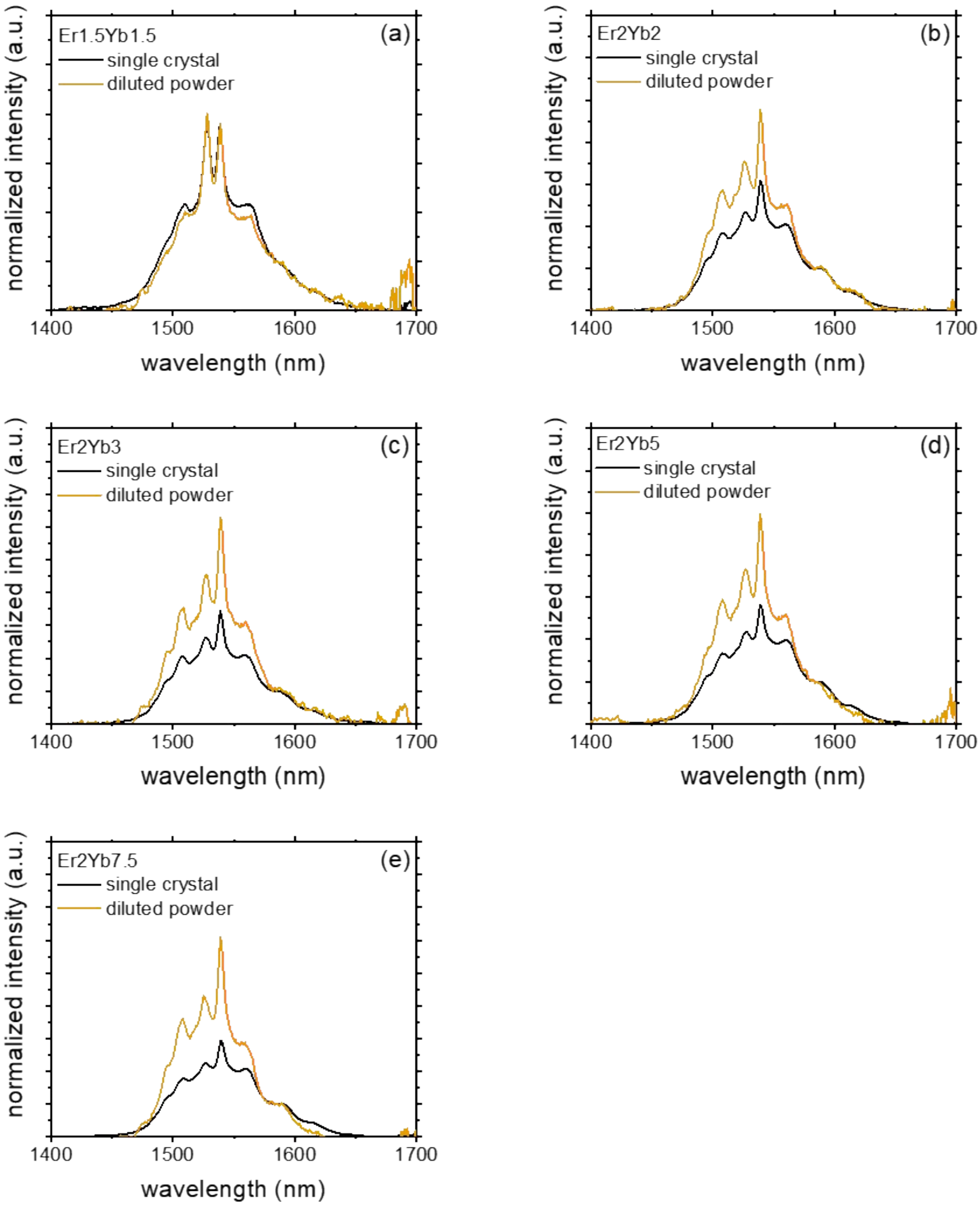

Figure S4.3. NIR range emission spectra of the single crystals and 9/1 diluted powders of the PbF_2:Er,Yb samples measured under 378 nm excitation with a spectrofluorometer (FS5, Edinburgh Instruments).

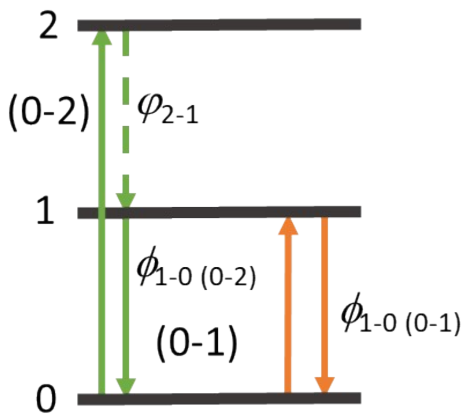

Figure S5. Energy transfer diagrams for the case of DS emission, where the ground state **0** is Er^{3+}:$^4I_{15/2}$, excited state **1** is either Er^{3+}:$^4I_{13/2}$ or Er^{3+}:$^4I_{9/2}$ and excited state **2** is either Er^{3+}:$^4I_{11/2}$ or Er^{3+}:$^4S_{3/2}$

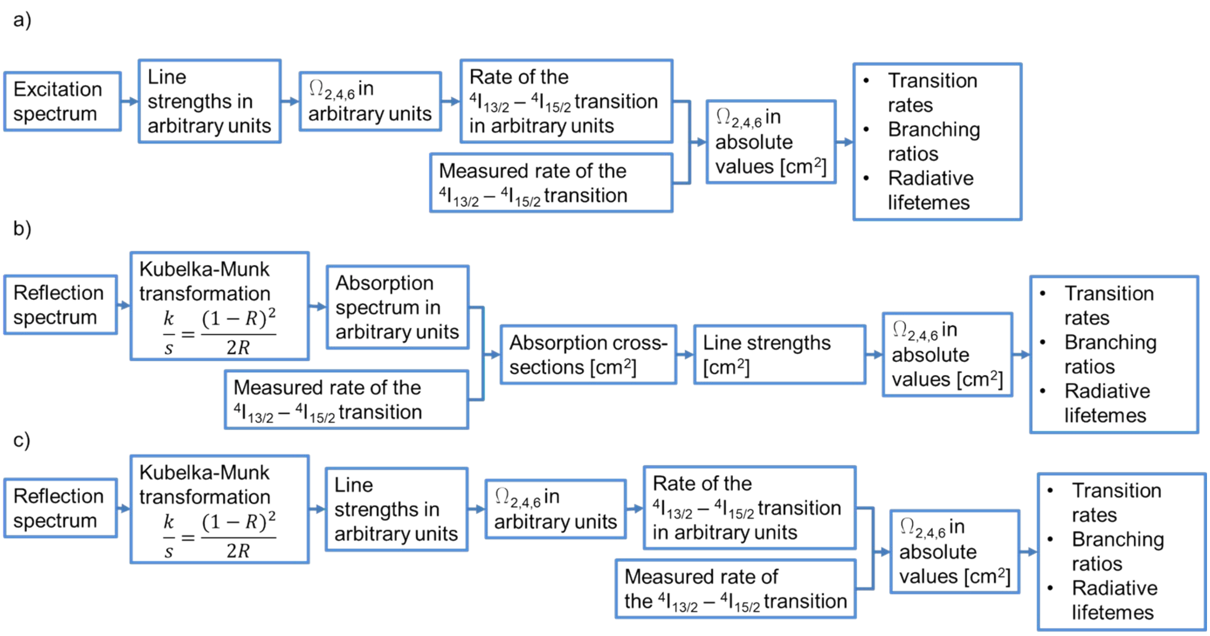

Figure S6. Different algorithms of JO calculation in the case of powder samples a) paper [3]; b) paper [4]; c) papers [5, 6]

Table S10. The comparison of branching ratios of Er2Yb5 powder obtained with different methods.

Emission band	**Lifetime, ms**			
	Crystal	*Method A* [3]	*Method B* [4]	*Method C* [5, 6]
$^4G_{9/2} – ^4I_{15/2}$	0.42	0.52	0.52	0.42
$^2H_{11/2} – ^4I_{15/2}$	0.97	0.97	0.97	0.97
$^4S_{3/2} – ^4I_{15/2}$	0.67	0.67	0.67	0.66
$^4F_{9/2} – ^4I_{15/2}$	0.91	0.88	0.88	0.93
$^4I_{9/2} – ^4I_{15/2}$	0.83	0.24	0.22	0.83
$^4I_{11/2} – ^4I_{15/2}$	0.73	0.89	0.78	0.73
$^4I_{13/2} – ^4I_{15/2}$	1	1	1	1
Relative RMS (with 4I9/2)		**0.26**	**0.68**	**0.68**
Relative RMS (w/o 4I9/2)		**0.12**	**0.19**	**0.11**

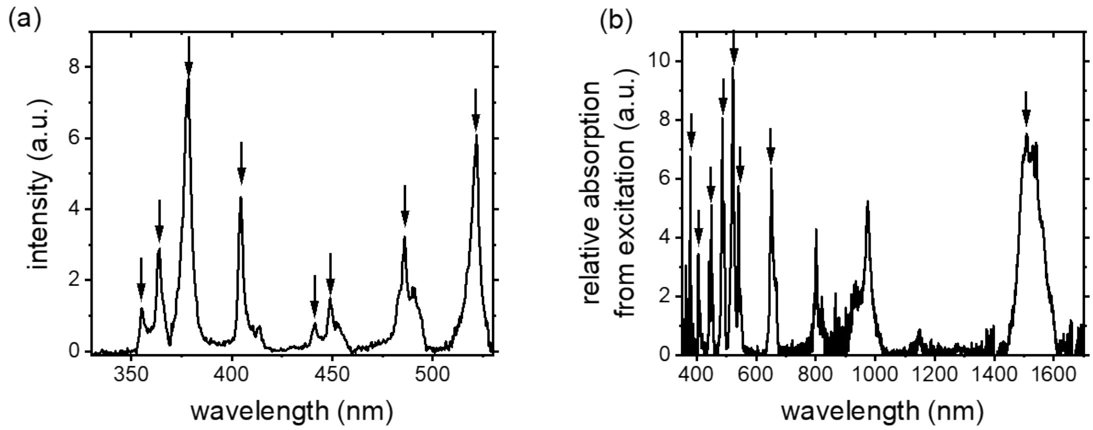

Figure S7. a) the excitation spectrum of the $^4S_{3/2} - ^4I_{15/2}$ transition (detection at 540 nm); b) the reflectance spectrum of the Er2Yb2 powder sample.

Table S11. The comparison of Ω_t parameters of Er2Yb2 powder obtained with different methods.

	Crystal	***Method A*** [3]	***Method B*** [4]	***Method C*** [5, 6]
$\mathbf{\Omega_2}$	1.34×10^{-20}	2.73×10^{-20}	1.60×10^{-20}	1.72×10^{-21}
$\mathbf{\Omega_4}$	4.70×10^{-21}	4.43×10^{-20}	7.43×10^{-21}	7.96×10^{-21}
$\mathbf{\Omega_6}$	1.79×10^{-20}	2.23×10^{-20}	2.34×10^{-20}	2.54×10^{-20}
Relative RMS		8.50	0.69	0.86

Table S12. The comparison of radiative lifetimes of Er2Yb2 powder obtained with different methods.

Emission band	**Lifetime, ms**			
	Crystal	*Method A* [3]	*Method B* [4]	*Method C* [5, 6]
$^4G_{9/2} - {}^4I_{15/2}$	0.59	0.43	0.56	0.52
$^2H_{11/2} - {}^4I_{15/2}$	0.61	0.35	0.84	0.78
$^4S_{3/2} - {}^4I_{15/2}$	0.85	0.73	0.69	0.65
$^4F_{9/2} - {}^4I_{15/2}$	1.14	0.64	1.42	1.32
$^4I_{9/2} - {}^4I_{15/2}$	9.47	4.93	13.99	12.75
$^4I_{11/2} - {}^4I_{15/2}$	9.26	8.21	8.83	7.70
$^4I_{13/2} - {}^4I_{15/2}$	8.39	8.39	12.31	8.39
Relative RMS (with 4I9/2)		0.84	0.83	0.57
Relative RMS (w/o 4I9/2)		**0.69**	**0.68**	**0.45**

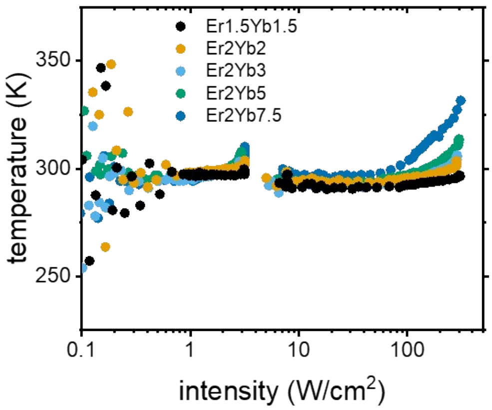

Figure S8. Sample temperature as a function of incident 976 nm intensity.

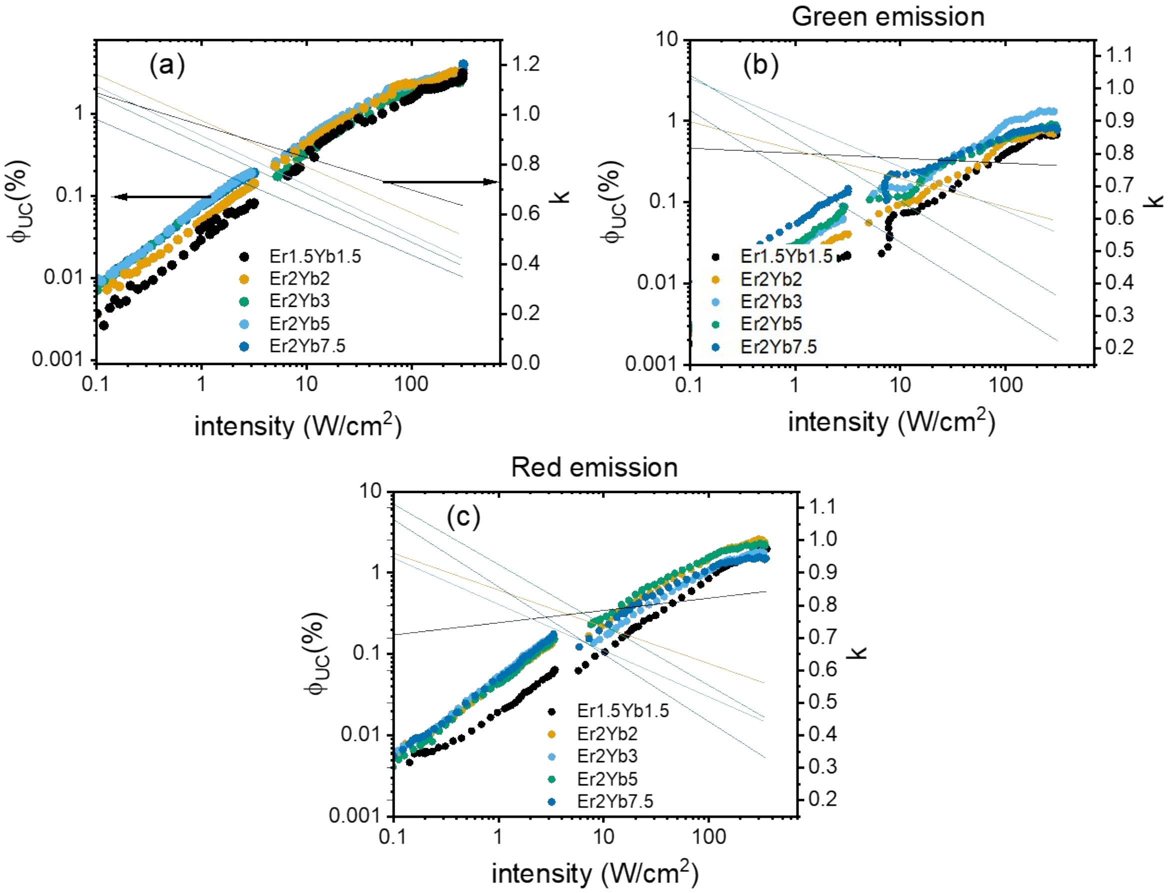

Figure S9. Measured ϕ_{UC} and slopes (k) of the ϕ_{UC} dependence of a) total UC emission in the 400 – 900 nm range, b) emission of the $^4S_{3/2} – ^4I_{15/2}$ transition, c) emission of the $^4F_{9/2} – ^4I_{15/2}$ transition in the intensity range of 0.1 – 350 W/cm^2.

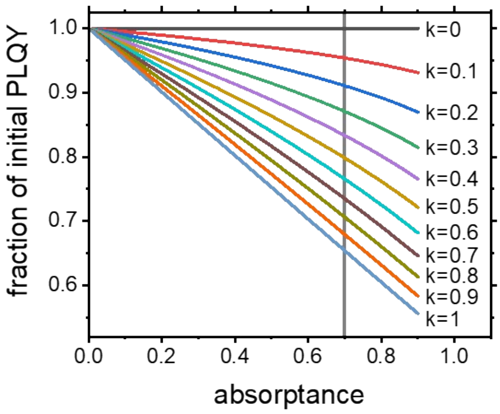

Figure S10. Relative change in ϕ_{UC} of a sample versus total absorptance and slope (k) of the ϕ_{UC} intensity dependence.

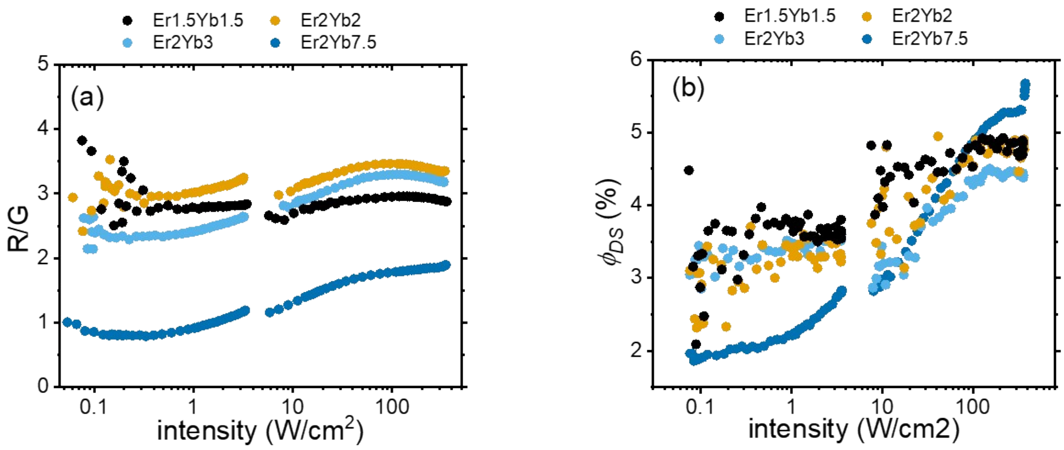

Figure S11. (a) Ratio of the intensities of the $^4F_{9/2}$ – $^4I_{15/2}$ (Red) transition and the $^4S_{3/2}$ – $^4I_{15/2}$ (Green) transition as a function of 976 nm excitation intensity in the 0.1 – 350 W/cm^2; (b) ϕ_{DS} of the Er^{3+}:$^4I_{13/2}$ – $^4I_{15/2}$ transition as a function of intensity at 940 nm excitation.

References

1. C. de Mello Donegá, A. Meijerink and G. Blasse, *J. Lumin.*, 1994, **62**, 189-201.
2. L. R. Wilson and B. S. Richards, *Appl. Opt.*, 2009, **48**, 212-220.
3. W. Luo, J. Liao, R. Li and X. Chen, *PCCP*, 2010, **12**, 3276-3282.
4. Y. Zhang, B. Chen, S. Xu, X. Li, J. Zhang, J. Sun, X. Zhang, H. Xia and R. Hua, *PCCP*, 2018, **20**, 15876-15883.
5. E. Cantelar, M. Marin-Dobrincic, T. Jardiel, A. C. Caballero and F. Cussó, *Opt. Mater.*, 2015, **41**, 122-125.
6. A. Egaña, M. Tardío, C. de la Torre-Gamarra, A. Várez, E. Cantelar and J. E. Muñoz Santiuste, *J. Lumin.*, 2018, **202**, 232-238.